

NUMERICAL STUDY OF LIQUID COMPOSITE MOLDING USING A SMOOTHED PARTICLE HYDRODYNAMICS METHOD

Di Su, Ronghui Ma,* & Liang Zhu

Department of Mechanical Engineering, University of Maryland Baltimore County, 1000 Hilltop Circle, Baltimore, MD 21250

*Address all correspondence to Ronghui Ma E-mail: roma@umbc.edu

Original Manuscript Submitted: 8/20/2010; Final Draft Received: 3/7/2011

Liquid composite molding is an important manufacturing process for a variety of composite components. The motion of fluid in a porous preform during a mold-filling process plays an important role in determining the quality of the composite part. In this study, a smoothed particle hydrodynamics (SPH) model is developed based on the Brinkman-Forchheimer-Darcy equation to study the mold-filling process with a special emphasis on the effects of operational conditions on the distributions of the fluid in the preform. The capillary pressure, which is important for a metal-based composite, is included in the model using the continuum surface force method. Two-dimensional simulations were performed to examine the effects of infusion rate, multiple infusion gates, and capillary pressure on the filling process. The results suggest that the SPH model provides an effective tool with sufficient accuracy for simulation, design, and optimization of mold filling for complex components.

KEY WORDS: liquid composite molding, smoothed particle hydrodynamics, free surface flow, capillary pressure, continuum surface force method

1. INTRODUCTION

Liquid composite molding (LCM) is a commonly used manufacturing process for fiber-reinforced, low-weight, and high-strength composites that are extensively used in many areas such as sporting goods, defense, automotive, and aerospace. LCM includes resin transfer molding, vacuum assisted resin transfer molding, structural reaction injection molding, etc. (Trochu et al., 2006). In LCM, liquid resin is forced to infiltrate through a porous preform placed inside a closed rigid mold by an external pressure or suction. The filling process involves a fluid infiltration in porous materials with a free moving front. After the mold-filling process, a cure process is initiated and the resin reacts into a cross-linked network (Shojaei et al., 2003). The manufacturing of high-quality composite parts requires a well-controlled fluid infiltration in the

preform to achieve a rapid yet steady filling of the mold and a complete expulsion of air. Inadequate design and control of the filling process may cause nonuniform distribution of the fluid and formation of voids (Pillai, 2004). The behavior of the fluid infiltration is affected by a number of parameters, such as infusion rates, the properties of the fluids and porous preforms, the arrangement of air vents and injection gates, and the deformation of the preform. A thorough understanding of the fluid transport in the preform and quantitative information on the location and shape of the flow front during the filling process is critical for a better design and optimization of an LCM process.

Numerical simulation has demonstrated to be a powerful tool for investigating the behavior of resin flow, optimizing the filling process, and designing the control algorithm (Johnson and Pitchumani, 2007; Nielsen and

NOMENCLATURE

<p>a acceleration vector</p> <p>Bo Bond number</p> <p>Ca capillary number</p> <p><i>c</i> color function</p> <p><i>c_s</i> speed of sound</p> <p><i>f</i> field function</p> <p><i>F</i> force</p> <p>g gravitational acceleration vector</p> <p><i>h</i> smooth length</p> <p><i>K</i> permeability of the porous media</p> <p><i>L</i> characteristic length</p> <p><i>m</i> mass</p> <p>n unit vector</p> <p><i>p</i> fluid pressure</p> <p><i>p_c</i> capillary pressure</p> <p><i>q</i> infusion rate</p> <p><i>r</i> radius</p> <p><i>t</i> time</p> <p>u average fluid velocity vector</p> <p><i>U</i> characteristic velocity</p>	<p><i>V</i> volume of the mold</p> <p><i>W</i> kernel function</p> <p>x position vector</p> <p>Greek Symbols</p> <p>γ surface tension coefficient</p> <p>δ Dirac delta function</p> <p>δ_s surface delta function</p> <p>ε porosity of the porous media</p> <p>θ contact angle</p> <p>μ dynamic viscosity</p> <p>ρ density</p> <p>σ stress tensor</p> <p>ϕ viscous strain rate</p> <p>Subscripts</p> <p>f fluid</p> <p>c capillary</p> <p><i>i, j</i> particle index</p> <p>Superscripts</p> <p>α, β coordinate direction</p>
---	---

Pitchumani, 2002; Hsiao and Advani, 2004; Devillard et al., 2005; Hsiao et al., 2004). In most of the numerical simulations, preforms are assimilated to porous media and the mold-filling process is modeled as resin flow in an unsaturated porous medium with a moving flow front. A comprehensive review of the numerical methods for molding filling can be found in Trochu et al. (2006). The finite element with control volume (FE/CV) method has been widely used to investigate the resin flow in the LCM process (Trochu et al., 1993; Kelly and Bickerton, 2009). A major challenge for the traditional methods based on fixed meshes is the complex algorithm to track the moving interface (Tezduyar, 2001; Sethian and Smereka, 2003). Meshless methods, such as the lattice Boltzmann and smoothed particle hydrodynamics (SPH) method, have emerged as novel modeling tools in this area due to their ability to handle moving interface with large deformation

without the need of interface tracking (Trochu et al., 2006; Cleary et al., 2007; Comas-Cardona et al., 2005). Sawley et al. (1999) developed a pore-scale SPH model to study resin flow through the pores of a porous medium, and investigated the effect of the edge flow. Although the model gave good qualitative results, it is difficult to simulate the filling process at a mold scale using the pore-scale simulation. Comas-Cardona et al. (2005) used coupled FE-SPH to simulate the hydromechanical coupling process.

In this study, we conducted 2D simulations of LCM using the SPH method. The Brinkman-Forchheimer-Darcy equation is employed to describe the fluid infiltration because of its ability to address a large variety of flows in porous media. The capillary force on the flow front was included in this model using the continuum surface force (CSF) method so that the model can be applied to metal-based composite parts. The model was used to study the

effects of operation parameters, such as infusion rate, multigate infusion, and capillary pressure, on the filling process in molds of various geometries.

2. MATHEMATICAL MODEL

2.1 Governing Equations

We consider that the fluid is isothermal, incompressible, and Newtonian, and the porous medium is isotropic, homogeneous, and nondeformable (Bickerton et al., 2000; Comas-Cardona et al., 2005; Dai et al., 2004; Pillai, 2004). It is also assumed that the liquid phase is free of additives, voids, and chemical reactions between the fluid and solid phase. The liquid phase is fully saturated, and is the only phase considered in this simulation, which implies that air in the mold can be expelled expediently through the air vents.

Existing studies of mold-filling processes have suggested that Darcy's equation is sufficient to describe resin flow in the preforms (Shojaei et al., 2003). However, it does not consider the effects of viscous drag due to the solid boundary and inertia force, which might be important for applications such as fluid flow in biological tissues or high-velocity flows through porous media (Vafai and Tien, 1981). In order to develop an SPH model that is not only suitable for mold filling but also has the potential to address a broad range of applications, we employed the Brinkman-Forchheimer-Darcy equation, which includes the effects of impermeable boundaries and inertia (Vafai and Tien, 1981). The continuity and generalized Brinkman-Forchheimer-Darcy equations are

$$\frac{\partial}{\partial t}(\rho_f) + \nabla \cdot (\rho_f \mathbf{u}) = 0 \quad (1)$$

$$\frac{\rho_f}{\varepsilon} \left[\frac{\partial \mathbf{u}}{\partial t} + (\mathbf{u} \cdot \nabla) \mathbf{u} \right] = -\nabla p + \frac{\mu}{\varepsilon} \nabla^2 \mathbf{u} + \rho_f \mathbf{g} - \frac{\mu}{K} \mathbf{u} - \frac{\rho_f F_{iner} \varepsilon}{\sqrt{K}} [\mathbf{u} \cdot \mathbf{u}] \mathbf{J} \quad (2)$$

where \mathbf{u} is the average fluid velocity vector, p is the average pressure, ε is the porosity, ρ_f and μ are the fluid density and viscosity, respectively, t is the time, K is the permeability of the porous medium, F_{iner} is the dimensionless inertia term coefficient, \mathbf{g} is the gravitational acceleration vector, and $\mathbf{J} = \mathbf{u}/|\mathbf{u}|$ is a unit vector oriented along the velocity vector. The last term on the right-hand side of Eq. (2) refers to the inertial effects. The significance of inertia can be evaluated by the Reynolds number, which is defined as $Re = \rho_f U d_p / \mu$, where U is the

fluid velocity, and d_p is the representative grain diameter of the porous medium. When $Re \ll 10$, which is the case for mold filling, fluid inertia becomes inappreciable (Hsu and Cheng, 1990); thereby, the last term on the right-hand side of Eq. (2) is neglected.

2.2 Boundary Conditions

The resin flow during a mold-filling process is a free surface flow with one or more interfaces with the air in the porous preform. As the fluid wets the porous matrix, the meniscus can be either concave or convex, depending on the wetting properties of the fluid on the solid. The surface tension of the fluid exerts an extra force that either favors or resists the motion of the fluid. Typically, this interaction is considered as the capillary pressure p_c acting in the direction normal to the interface. The capillary pressure is dependent on the average pore size, wetting property of the liquid on the solid, and surface tension coefficient of the fluid. In an idealized capillary tube, the capillary pressure is (Dullien, 1992)

$$p_c = -\frac{2\gamma \cos \theta}{r_c} \quad (3)$$

where γ is the surface tension coefficient of the fluid, θ is the contact angle, and r_c is the radius of the capillary tube. For flows in porous media, r_c is taken as the average radius of the pores, which is related to the porosity and permeability through the equation (Kopenon et al., 1997)

$$r_c = \sqrt{\frac{8K}{\varepsilon}} \quad (4)$$

Note that when the contact angle is <90 deg, the meniscus formed inside a capillary tube is concave and the capillary pressure tends to pull the liquid front into the porous material; otherwise, there exists a resistance to the motion of the liquid. Two dimensionless numbers, capillary number (Ca) and Bond number (Bo), are used to compare the magnitude of capillary pressure with viscous force and gravitational body force, respectively. With U defined as the characteristic velocity and L as the characteristic length (the radius of a pore for porous media), the capillary and Bond numbers have, respectively, the expressions of

$$Ca \equiv \frac{\mu U}{\gamma}, \quad Bo \equiv \frac{\rho g L^2}{\gamma} \quad (5)$$

Fluid flow in porous media is dominated by the capillary force when $Ca \ll 10^{-5}$ and/or $Bo < 1$.

In a mold-filling process, the air is assumed to have negligible influence on the motion of the fluid, thus the tangential component of the viscous stress is zero on the free boundary. The normal stress on the free surface is determined by the pressure of the environment p_s and the capillary pressure p_c ,

$$\sigma_n = -(p_s + p_c)\hat{\mathbf{n}} \quad (6)$$

where σ_n is the normal component of the stress tensor on the free surface, and $\hat{\mathbf{n}}$ is the unit vector normal to the free surface. No-slip conditions and constant infusion velocity are used for mold surfaces and the infusion gate, respectively.

2.3 SPH Method and SPH Equations

The governing equations (1) and (2) are solved numerically using the SPH method. The SPH method and its modified versions have been widely used in hydrodynamics, heat transfer, and mechanics (Liu and Liu, 2003). Unlike traditional FE/FV methods, a continuum medium in the SPH is represented by a set of discrete particles, each particle having a mass m , a density ρ , a velocity \mathbf{v} , a position vector \mathbf{x} , and other quantities. The particles interact with each other, and the evolutions of the density, velocity, and position with time are governed by the hydrodynamic equations written in the SPH form. The basic concept of the SPH is that a function can be approximated as summation of interpolants using a kernel function W with a smoothing length h . The SPH approximations of a field function f and its first derivative at particle i are

$$\langle f_i \rangle = \sum_{j=1}^N \frac{m_j}{\rho_j} f_j W_{ij} \quad (7)$$

$$\langle \nabla f_i \rangle = \sum_{j=1}^N \frac{m_j}{\rho_j} f_j \nabla_i W_{ij} \quad (8)$$

respectively, where j represents the neighboring particles within the smoothing length h ; m_j and ρ_j are the mass and density of particle j ; W and ∇W are the kernel function and the gradient of the kernel function at i , respectively; and N is the total number of the particles within the influence domain that contribute to the value of f at particle i . Approximation of higher-order derivatives can be carried out by nested approximation using lower-order derivatives. Among various forms of the kernel functions, we chose the quartic kernel function in this study because of its good accuracy and stability (Monaghan, 1992; Liu

and Liu, 2003). A quartic kernel function takes the form of

$$W(s, h) = \alpha_d \begin{cases} \left(\frac{2}{3} - \frac{9}{8}s^2 + \frac{19}{24}s^3 - \frac{5}{32}s^4 \right) & 0 \leq s \leq 2 \\ 0 & 0 \\ s > 2 \end{cases} \quad (9)$$

where $s = |\mathbf{x}_i - \mathbf{x}_j|/h$, s is the relative distance between two particles at the positions of i and j , and α_d takes the value of $15/7\pi h^2$ and $315/208\pi h^3$ for two and three dimensions, respectively.

The derivation of SPH formulations for the continuity and Navier-Stokes equations is demonstrated clearly in Liu and Liu (2003). Using the same SPH particle approximation, the Brinkman-Forchheimer-Darcy and continuity equations can be reformulated as (Liu and Liu, 2003)

$$\begin{aligned} \frac{D\mathbf{u}_i^\alpha}{Dt} = & -\varepsilon_i \sum_j m_j \left(\frac{p_i}{\rho_i^2} + \frac{p_j}{\rho_j^2} \right) \frac{\partial W_{ij}}{\partial \mathbf{x}_i^\alpha} \\ & + \sum_j m_j \left(\frac{\mu_i \varphi_i^{\alpha\beta}}{\rho_i^2} + \frac{\mu_j \varphi_j^{\alpha\beta}}{\rho_j^2} \right) \frac{\partial W_{ij}}{\partial \mathbf{x}_i^\beta} \\ & - \frac{\varepsilon_i}{K_i \rho_i} \sum_j \frac{\mu_j m_j}{\rho_j} \mathbf{u}_j^\alpha W_{ij} + \varepsilon_i \mathbf{g} + \frac{\varepsilon_i}{\rho_i} \mathbf{f}_s \end{aligned} \quad (10)$$

$$\frac{D\rho}{Dt} = \sum_j m_j (\mathbf{u}_i - \mathbf{u}_j) \cdot \frac{\partial W_{ij}}{\partial \mathbf{x}_i^\beta} \quad (11)$$

where the Greek superscripts α and β denote the coordinate directions, $\varphi^{\alpha\beta}$ is the viscous strain rate, and \mathbf{f}_s is the volumetric body force, which is added in the equation to handle the capillary pressure on the interface (Morris, 2000). The viscous strain rate $\varphi^{\alpha\beta}$ is expressed as (Liu and Liu, 2003)

$$\begin{aligned} \varphi_i^{\alpha\beta} = & \sum_j \frac{m_j}{\rho_j} \mathbf{u}_{ji}^\beta \frac{\partial W_{ij}}{\partial \mathbf{x}_i^\alpha} + \sum_j \frac{m_j}{\rho_j} \mathbf{u}_{ji}^\alpha \frac{\partial W_{ij}}{\partial \mathbf{x}_i^\beta} \\ & - \left(\frac{2}{3} \sum_j \frac{m_j}{\rho_j} \mathbf{u}_{ji} \nabla_i W_{ij} \right) \delta^{\alpha\beta} \end{aligned} \quad (12)$$

where δ is the Dirac delta function. An artificial state equation based on the idea that a theoretically incompressible flow is practically compressible is widely used to compute the pressure in the SPH method, which is

$$p = c_s^2 (\rho - \rho_0) \quad (13)$$

where ρ_0 is the reference density of the fluid and c_s is the speed of the sound. The sound speed c_s must be chosen carefully to ensure a stable and accurate solution of a given problem (Morris, 2000). Typically, it should be chosen according to

$$(c_s^2) \sim \max \left(\frac{U^2}{\zeta}, \frac{\mu U}{\rho L \zeta}, \frac{FL}{\zeta} \right) \quad (14)$$

where $\zeta = \Delta\rho/\rho_0$, U and L are the characteristic velocity and length, respectively, and F is the magnitude of the body force (Liu and Liu, 2003).

3. NUMERICAL IMPLEMENTATION

The flow of resin in a porous medium is simulated by updating the density, pressure, velocity, and position of each particle at each time step following the algorithm presented in Fig. 1. The density and pressure are obtained by numerical integration of Eqs. (11) and (13) over a time step Δt . The velocity and position of each particle are

updated using the predictor-corrector integration scheme, which is as follows:

$$\mathbf{u}_{i,t+\Delta t/2}^p = \mathbf{u}_{i,t} + \frac{1}{2} \mathbf{a}_{i,t} \Delta t \quad (15a)$$

$$\mathbf{x}_{i,t+\Delta t/2}^p = \mathbf{x}_{i,t} + \frac{1}{2} \mathbf{u}_{i,t} \Delta t \quad (15b)$$

where p designates the predictor. With the predicted velocity and position vectors at the half time step, the acceleration of particle i at the half time step, $\mathbf{a}_{i,t+\Delta t/2}$, can be computed using Eq. (10). The particle velocity and position vector can then be corrected by

$$\mathbf{u}_{i,t+\Delta t/2}^c = \mathbf{u}_{i,t} + \frac{1}{2} \mathbf{a}_{i,t+\Delta t/2} \Delta t \quad (16a)$$

$$\mathbf{x}_{i,t+\Delta t/2}^c = \mathbf{x}_{i,t} + \frac{1}{2} \mathbf{u}_{i,t+\Delta t/2}^c \Delta t \quad (16b)$$

where c designates the corrector estimates. Finally, the velocity and position vectors at the end of each time step can be calculated as

$$\mathbf{u}_{i,t+\Delta t} = 2\mathbf{u}_{i,t+\Delta t/2}^c - \mathbf{u}_{i,t} \quad (17a)$$

$$\mathbf{x}_{i,t+\Delta t} = 2\mathbf{x}_{i,t+\Delta t/2}^c - \mathbf{x}_{i,t} \quad (17b)$$

According to the Courant-Friedrichs-Levy (CFL) condition, the time step is proportional to the smallest particle resolution (Liu and Liu, 2003), i.e., $\Delta t \sim \min(h_i/c_s)$.

4. NUMERICAL TREATMENT OF CAPILLARY FORCE ON THE MOVING INTERFACE

The existing studies of mold filling using SPH are limited to zero capillary force on the flow front, which is not applicable to metal-based composites where the effect of capillary force may be important (Michaud and Moresen, 2001). In a case where the surface force and tangent component of the viscous stress are zeroes, the nature of the SPH method allows the motion of the free boundary to be simulated straightforwardly. However, the presence of the capillary pressure requires a special treatment of the surface force. In this study, the CSF method is used to translate the surface pressure into a volumetric force \mathbf{f}_s exerted on the particles located on the free surface (Brackbill et al., 1992). It is expressed as

$$\mathbf{f}_s = \mathbf{p}_c \delta_s \quad (18)$$

where \mathbf{p}_c is the capillary pressure on the free surface calculated by Eq. (3), and δ_s is a surface delta function that

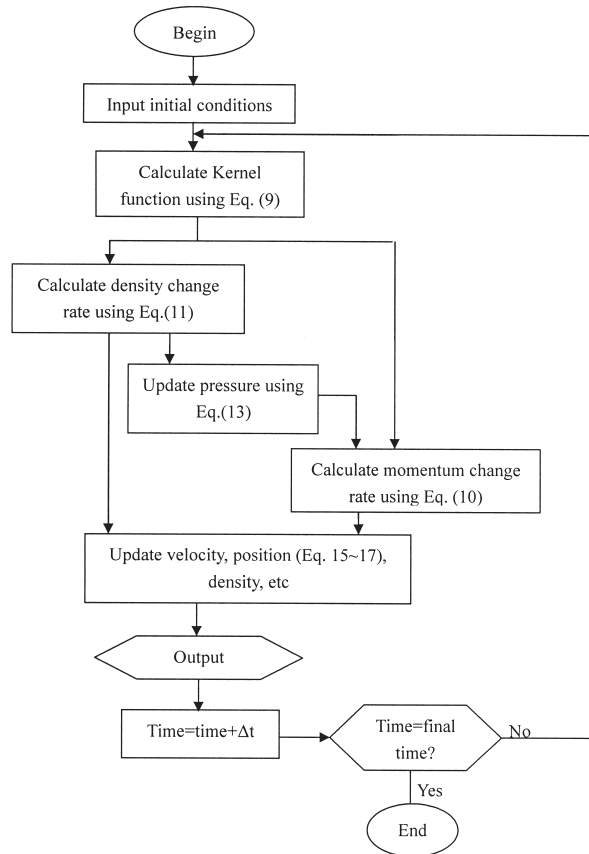


FIG. 1: Flowchart of the SPH solution algorithm.

peaks at the interface. The integral of δ_s across the boundary must be unity. To evaluate δ_s at the flow front, the color function method and virtual particles are used in the numerical algorithm. As shown in Fig. 2, a number of virtual particles of the same density as the fluid are deployed outside the flow front. The virtual fluid particles move with the fluid but do not affect the motion and properties of the fluid particles. A color function “ c ” is used to distinguish different types of particles, which is $c_i = 1$ for the fluid particles and $c_i = 0$ for virtual particles (Morris, 2000). Based on the distribution of the color function, the surface normal function is evaluated as

$$\mathbf{n} = \sum_j \frac{m_j}{p_j} (c_j - c_i) \nabla_i W_{ij} \quad (19)$$

On the basis of the CSF method, $\delta_s = |\mathbf{n}|$ (Brackbill et al., 1992; Morris, 2000).

5. RESULTS AND DISCUSSIONS

5.1 Model Validation

The SPH model for the mold-filling process was validated by comparing flow front positions and relative inlet pressures obtained from analytical solution and numerical simulation. For a constant infusion rate, the filling time is calculated as (Dai et al., 2004)

$$t = \frac{\varepsilon V_{\text{mold}}}{q} \quad (20)$$

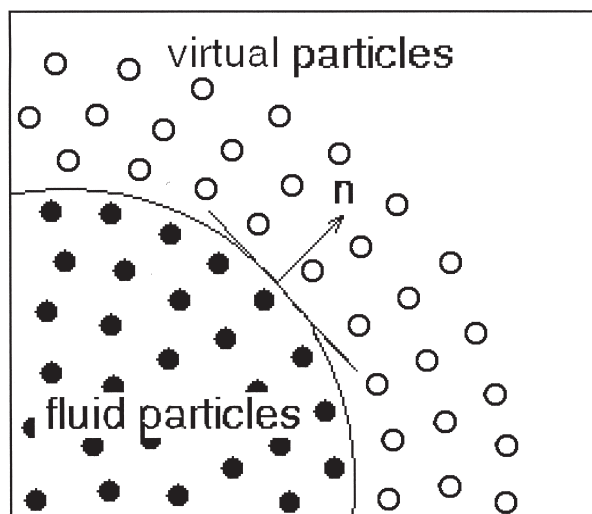


FIG. 2: Fluid and virtual particles used for the calculation of the surface delta function.

where V_{mold} is the volume of the mold, ε is the porosity of the composite matrix, and q is the constant infusion rate. When the effect of gravity and capillary pressure are neglected, the relative inlet pressure, which is the pressure difference between the inlet and the environment, is

$$P_{\text{inlet}} = -\frac{\varepsilon U \mu L}{K} \quad (21)$$

We performed a 1D simulation in a mold of 15 cm in length for two constant infusion velocities: 0.05 m/s and 0.1 m/s. The resin viscosity is 0.1 Pa s, and the porosity and permeability of the preform are 0.5 and 1×10^{-9} m², respectively. The time step used in this simulation is 4 μ s, and the total number of liquid particles is 1600. The variation of the fluid density in the computation is <3%. The effects of the gravity and capillary pressure were not considered.

Figures 3(a) and 3(b) show, respectively, the flow front positions for the inlet location of $x = 0$, and the relative inlet pressures as a function of time predicted by the analytical and numerical solutions. Both quantities increase linearly with time as predicted by the analytical solutions. The numerical results agree well with the analytical predictions.

6. SIMULATION OF MOLD-FILLING PROCESS

The primary objective of a mold-filling process is to achieve a complete and uniform filling of the mold, while minimizing the filling time and formation of voids and defects. Given a mold of specific size and shape, information on the spreading of resin is important for the design of the infusion gate, air vent location, and the selection of the infusion rate (Pillai, 2004). In this study, 2D simulations of the resin flow in thin composite parts were performed using the SPH model. For thin composite parts, only flow in the planar direction is considered.

6.1 Case 1. Single Gate Infusion

Figure 4(a) shows schematically the configuration of the molding filling with a single gate. The width of the gate is 2 cm and the mold size is $8 \times 3 \times 0.4$ cm. Air vents are positioned on the sides and bottom of the mold. The fluid and preform properties used in this study are given in Table 1. We used a time step of 4 μ s and a smooth length h of 0.1 cm in the SPH simulation. Total number of solid particles is 2400. Doubling the number of the particles leads to a global difference of <3% in the velocity

TABLE 1: Properties of resin and preform used in the simulation

Properties	Value	Reference
Resin viscosity (Pa·s)	0.1	Bickerton et al. (2000), Tan and Pillai (2008)
Infusion velocities (m/s)	0.05, 0.1	Elgafy and Lafdi (2007), Sawley et al. (1999)
Resin density (kg/m ³)	1400	Elgafy and Lafdi (2007), Lefevre et al. (2007)
Surface tension coefficient of resin (dnes/cm)	35	Gonçalves et al. (1997), Toy (1965)
Contact angle of resin on carbon fiber (deg)	40	Gonçalves et al. (1997), Toy (1965)
Preform porosity	0.5	Dai et al. (2004), Trochu et al. (2006), Tan and Pillai (2008) Young and Lai (1997)
Preform permeability (m ²)	10 ⁻⁹ –10 ⁻¹⁰	Bickerton et al. (2000), Elgafy and Lafdi (2007), Tan and Pillai (2008)
Material of preform	Carbon	Elgafy and Lafdi (2007)

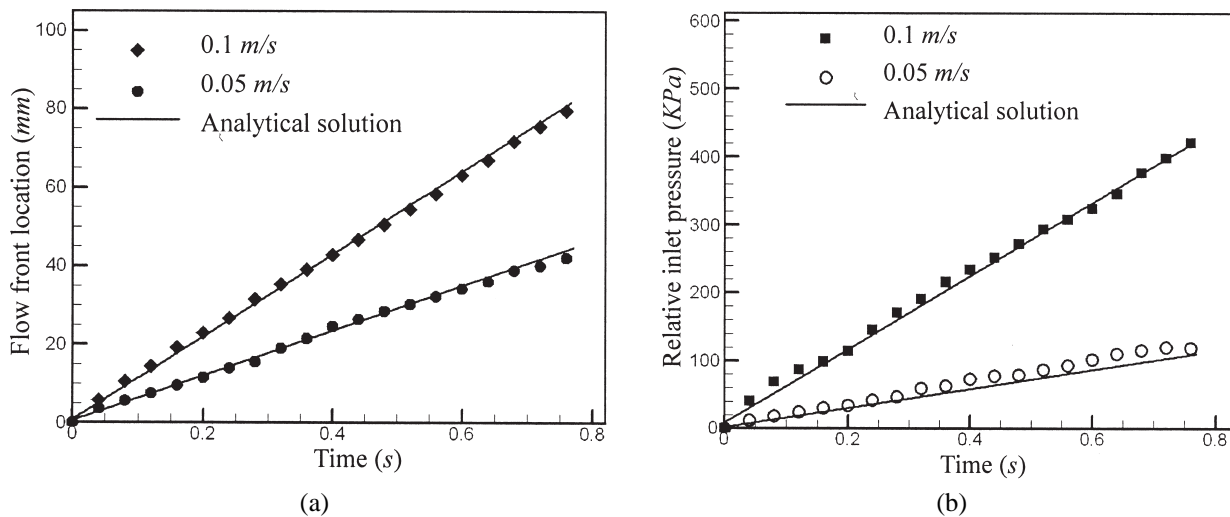


FIG. 3: (a) The variations of the flow front location with time for different infusion velocities; (b) the variations of the relative inlet pressure with time for different infusion velocities.

and pressure fields. The same numerical parameters are employed in cases 2 and 3.

The evolution of the flow front in the preform depicted in Fig. 4(b) shows that the flow is nearly isotropic before the flow front reaches the bottom of the mold. This is because the preform is assumed to be homogeneous. Figure 5 shows that the volume percentage occupied by the resin increases linearly with time, which agrees well with the analytical calculations (Dai et al., 2004; Shojaei et al., 2003). Figure 6 gives the histories of the relative inlet pressures for two infusion rates. The inlet pressures

increase nearly exponentially with time in order to maintain a constant infusion rate. Similar trends of the inlet pressure variation have been reported for a constant infusion rate (Comas-Cardona et al., 2005).

We performed 2D simulations with different infusion velocities of 0.005, 0.05, and 0.1 m/s to study how the infusion rate affects the flow front shape. Figure 7 depicts the shapes of the flow fronts when the center of the front advances to the same *y* location for different infusion velocities. Since a high infusion rate leads to a fast penetration of the fluid in the vertical direction within a short

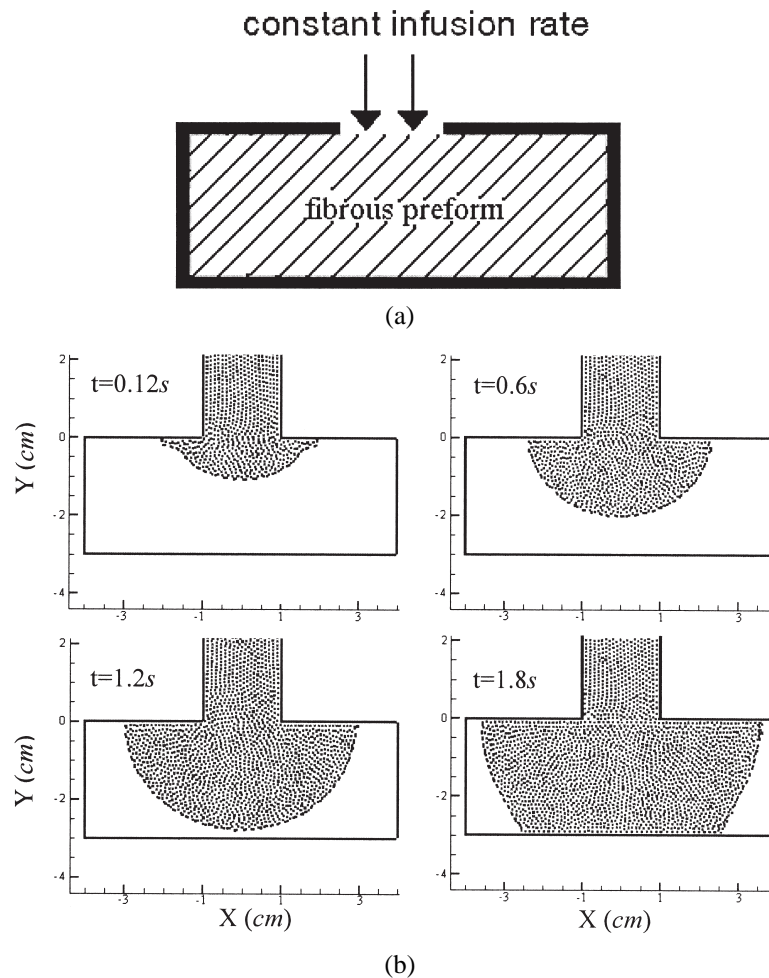


FIG. 4: (a) The schematic of the mold-filling process for the 2D SPH model; (b) the distributions of the resin flow in the mold.

filling time, it also results in a narrower spreading of the resin in the lateral direction; however, the difference in the spreading width is insignificant. A pronounced influence of the infusion rate on the front shape is anticipated when the preform is anisotropic and/or deformable.

6.2 Case 2. Multigate Infusion in a Mold of Complex Geometry

Multigate infusion is widely used in the LCM, especially for molds of complex geometries, to shorten the filling time, avoid the pressure buildup, and to yield uniform wetting of a preform (Dai et al., 2004; Kang et al., 2000). With more than one infusion gate, special attention is

needed when selecting the size and location of the infusion gates. The meshless nature of the SPH makes it a convenient tool for modeling the merge of the irregular-shaped flow fronts in a filling process. In this study, we simulated a mold filling process with single and multiple gates as shown in Figs. 8(a) and 8(b), respectively. The comb-shaped mold has three circular cavities and five branches. The size of the mold is $8 \times 6 \times 0.4$ cm, and the width of each gate is 1 cm. A constant infusion velocity of 0.05 m/s is imposed on each of the gates during the infusion. The evolutions of the resin distribution with single and triple gates are shown in Figs. 9(a) and 9(b), respectively. At the beginning of the filling process, the resin flows around the cavities, followed by a merge of the fluid before entering the branches. A single infusion gate

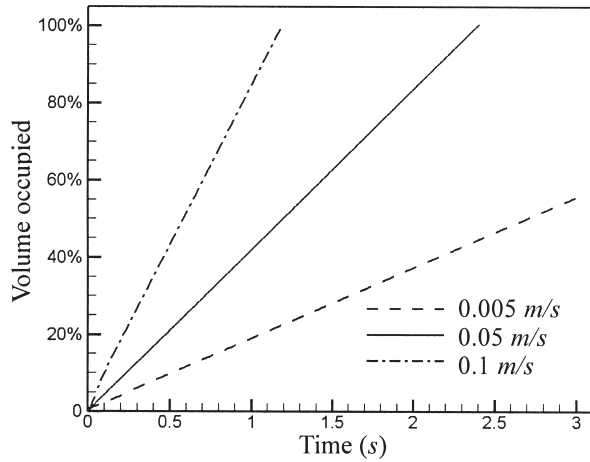


FIG. 5: The variations of resin-filled mold volume with time for different infusion velocities.

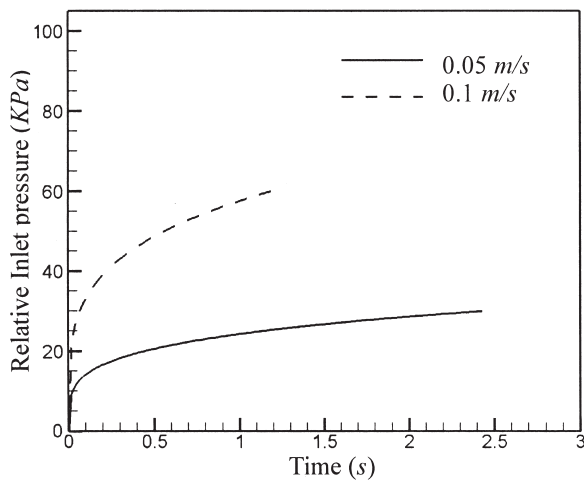


FIG. 6: The variations of relative inlet pressures with time for various infusion velocities.

causes the resin to infiltrate predominantly along the vertical centerline and favors the center branch. Consequently, the distributions of the resin in the branches are not uniform. When the resin is infused through three gates, a better resin distribution and a shorter infusion time are achieved. The pressures applied on the infusion gates are given in Fig. 10. It can be seen that a single gate infusion requires an increased pressure and extra time to fill the side branches at the end of the filling process. For multi-gate infusion, the pressure for the center gate is higher than the other two gates. The position and size of the gates can be adjusted to obtain an evenly distributed load and uniform wetting.

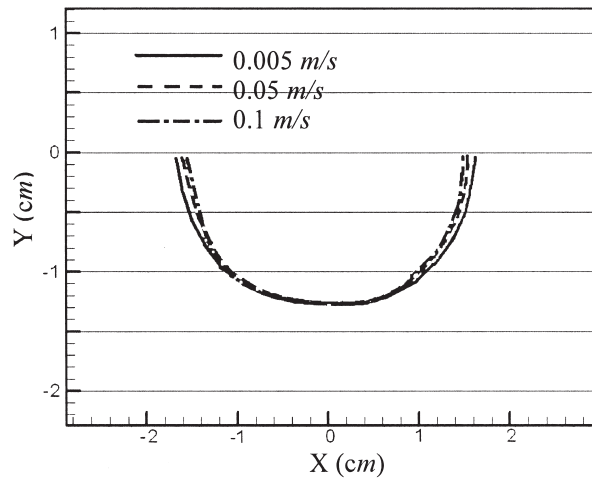


FIG. 7: The shapes of the flow front for various infusion velocities.

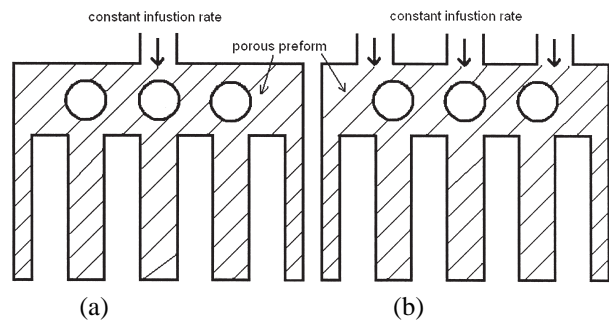


FIG. 8: The schematics of a comb-shaped mold with (a) single gate, and (b) multiple gates.

6.3 Case 3. Mold Filling with Capillary Pressure on the Flow Front

For typical resin infiltration conditions, the capillary pressure in the fiber preform under a low infusion rate usually is on the order of thousands of Pascals. The capillary number Ca is usually $> 10^{-5}$, and the Bond number Bo is greater than one, suggesting that the capillary pressure is not dominant. However, capillary pressure can be an important factor for metal-based infiltration because of the large surface tension coefficients of metal fluids (Michaud and Morensen, 2001). A typical capillary pressure can be as high as 10 MPa. We studied case 1 with the consideration of various capillary pressures on the flow front. Depicted in Fig. 11 are the evolutions of the inlet pressure with time for different capillary pressures. It is clear that

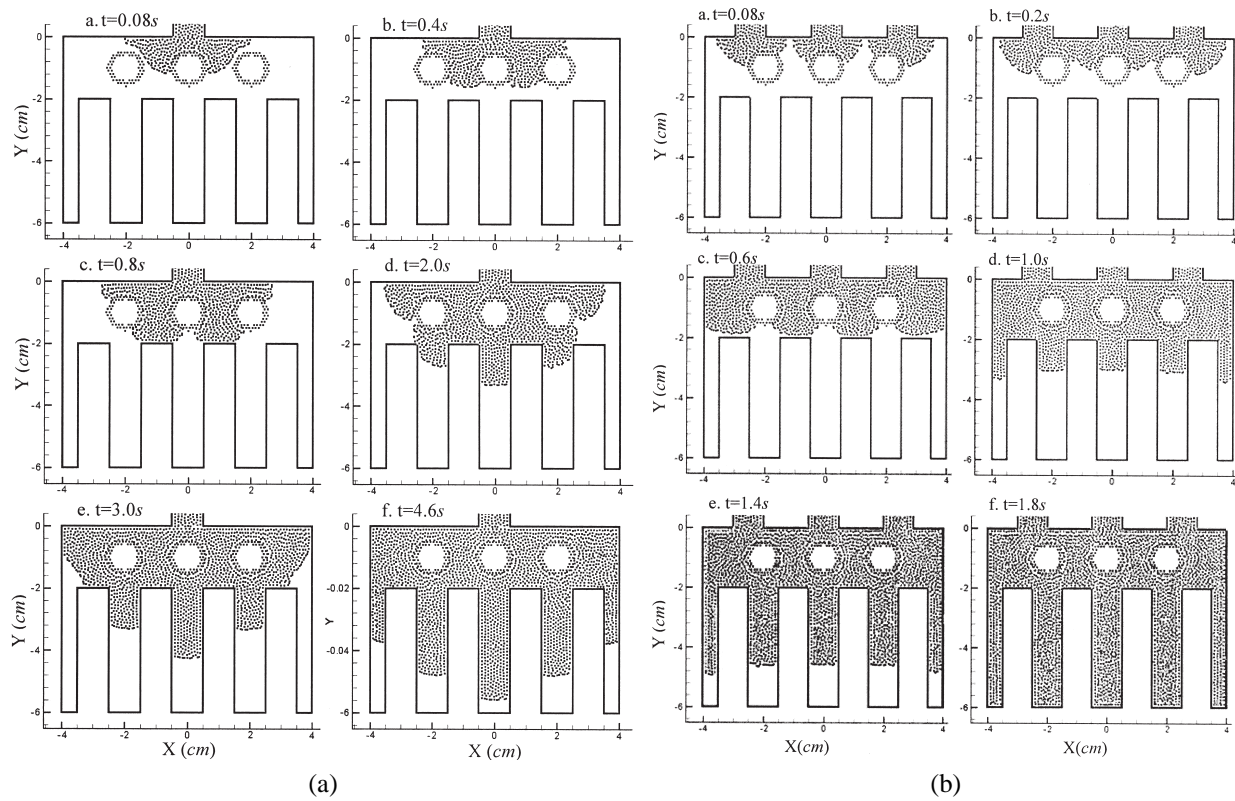


FIG. 9: (a) The evolution of the resin distribution for single gate infusion; (b) the evolution of the resin distribution in the mold for multigate infusion.

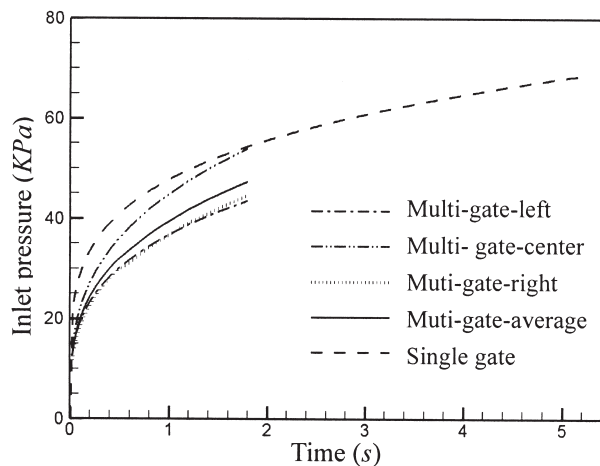


FIG. 10: The evolutions of the relative inlet pressures with time.

a high capillary pressure can significantly reduce the inlet pressure during the filling process for a constant infusion rate.

7. CONCLUSION

An SPH model was developed for studying the mold-filling process based on the Brinkman-Forchheimer-Darcy equation. The meshless and the adaptive nature of the SPH method enable the treatment of the free surface flow in a mold of complex geometry with great ease. The comparison of the numerical simulation with the analytical solution shows that the Brinkman-Forchheimer-Darcy equation is suitable for resin flow through porous media in a mold-filling process. Two-dimensional simulations were performed to study the effects of infusion rate and multigate infusion on the evolution of the resin distribution in a porous preform. This shows that the multigate injection provides an extra maneuverability of the fluid distribution and inlet pressure, but it requires careful design of the gate location and infusion rate. In addition, capillary pressure on the flow front is included in the SPH model using the CSF method, thus enabling the SPH model to be applied to a metal-based infiltration process. Since the numerical work presented in this pa-

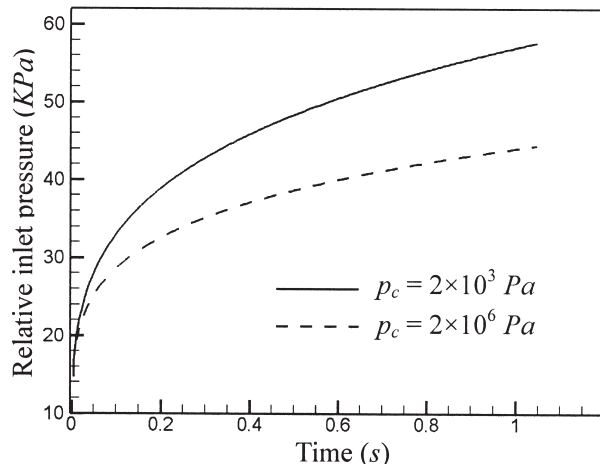


FIG. 11: The evolutions of the relative inlet pressure with time for different capillary pressures on the flow front (in-fusion velocity 0.1 m/s).

per is the first step of a systematical study of mold filling with the SPH method, the current study is limited to isothermal, homogeneous, isotropic, and nondeformable preforms. This study will continue by progressively including more features relevant to the physical phenomena associated with various types of LCM processes.

ACKNOWLEDGMENT

This research was partially supported by NSF Grants No. CBET-0730732 and No. CBET-0828728.

REFERENCES

- Bickerton, S., Advani, S. G., Mohan, R. V., and Shires, D. R., Experimental Analysis and Numerical Modeling of Flow Channel Effects in Resin Transfer Molding, *Polym. Compos.*, vol. **21**, pp. 134–153, 2000.
- Brackbill, J. U., Kothe, D. B., and Xemach, C., A Continuum Method for Modeling Surface Tension, *J. Comput. Phys.*, vol. **100**, pp. 335–354, 1992.
- Comas-Cardona, S., Groenenboom, P., Binetruy, C., and Krawczak, P., A Generic Mixed FE-SPH Method to Address Hydro-mechanical Coupling in Liquid Composite Moulding Processes, *Composites A*, vol. **36**, pp. 1004–1010, 2005.
- Cleary, P. W., Prakash, M., Ha, J., Stokes, N., and Scott, C., Smoothed Particle Hydrodynamics: Status and Future Potential, *Prog. Comput. Fluid Dyn.*, vol. **7**, pp. 70–90, 2007.
- Dai, F., Zhang, B., and Du, S., Analysis of Upper- and Lower-limits of Fill Time in Resin Transfer Mold Filling Simulation, *J. Compos. Mater.*, vol. **38**, pp. 1115–1136, 2004.
- Devillard, M., Hsiao, K.-T., and Advani, S. G., Flow Sensing and Control Strategies to Address Race-tracking Disturbances in Resin Transfer Molding, Part II: Automation and Validation, *Composites A*, vol. **36**, no. 11, pp. 1581–1589, 2005.
- Dullien, L. A. F., *Porous Media: Fluid Transport and Pore Structure*, 2nd ed., Academic Press, New York, 1992.
- Elgafy, A. and Lafdi, K., Engineering Solution in Monitoring Nanoparticle-Fluid Flow during Nanocomposites Processing, *J. Nanoparticle Res.*, vol. **9**, pp. 441–454, 2007.
- Goncalves, M., Pecora, J. D., Vinha, D., and Silva, R. S., Surface Tension of Different Dentin Bonding Resin Systems., *Braz. Dent. J.*, vol. **8**, pp. 43–47, 1997.
- Hsiao, K.-T. and Advani, S. G., Flow Sensing and Control Strategies to Address Race-Tracking Disturbances in Resin Transfer Molding. Part I: Design and Algorithm Development, *Composites A*, vol. **35**, no. 10, pp. 1149–1159, 2004.
- Hsiao, K.-T., Devillard, M., and Advani, S. G., Simulation Based Flow Distribution Network Optimization for Vacuum Assisted Resin Transfer Moulding Process, *Modell. Simul. Mater. Sci. Eng.*, vol. **12**, no. 3, pp. S175–S190, 2004.
- Hsu, C. T. and Cheng, P., Thermal Dispersion in a Porous Medium, *Int. J. Heat Mass Transfer*, vol. **33**, pp. 1587–1597, 1990.
- Johnson, R. J. and Pitchumani, R., Flow Control Using Localized Induction Heating in a VARTM Process, *Compos. Sci. Technol.*, vol. **67**, no. 3-4, pp. 669–684, 2007.
- Kang, M. K., Jung, J. J., and Lee, W., , Analysis of Resin Transfer Moulding Process with Controlled Multiple Gates Resin Injection, *Composites A*, vol. **31**, pp. 407–422, 2000.
- Kelly, P. A. and Bickerton, S., A Comprehensive Filling and Tooling Force Analysis for Rigid Mould LCM Processes, *Composites A*, vol. **40**, pp. 1685–1697, 2009.
- Kopenon, A., Kataja, M., and Timonen, J., Permeability and Effective Porosity of Porous Media, *Phys. Rev. E*, vol. **56**, pp. 3319–3325, 1997.
- Lefevre, D., Comas-Cardona, S., Binetruy, C., and Krawczak, P., Modelling the Flow of Particle-Filled Resin through a Fibrous Perform in Liquid Composite Molding Technologies, *Composites A*, vol. **38**, pp. 2154–2163, 2007.
- Liu, G. B. and Liu, M. B., *Smoothed Particle Hydrodynamics—A Meshfree Particle Method*, World Scientific, Singapore, 2003.
- Michaud, V. and Mortensen, A., Infiltration Processing of Fiber Reinforced Composites: Governing Phenomena, *Composites A*, vol. **32**, pp. 981–996, 2001.
- Monaghan, J. J., Smoothed Particle Hydrodynamics, *Ann. Rev. Astron. Astrophys.*, vol. **30**, pp. 543–574, 1992.
- Morris, J. P., Simulating Surface Tension with Smoothed Particle Hydrodynamics, *Int. J. Numer. Methods Fluids*, vol. **33**,

- pp. 333–353, 2000.
- Nielsen, D. R. and Pitchumani, R., Control of Flow in Resin Transfer Molding with Real-Time Preform Permeability Estimation, *Polym. Compos.*, vol. **23**, no. 6, pp. 1087–1110, 2002.
- Pillai, K. M., Modeling the Unsaturated Flow in Liquid Composite Molding Processes: A Review and Some Thoughts, *J. Compos. Mater.*, vol. **38**, pp. 2097–2118, 2004.
- Sawley, M. L., Cleary, P. W., and Joseph, H. A., Modeling of Flow in Porous Media and Resin Transfer Moulding Using Smoothed Particle Hydrodynamics, *Proceedings of the 2nd International Conference on CFD in the Minerals and Process Industries*, December 6–8, Melbourne, 1999.
- Sethian, J. A. and Smereka, P., Level Set Method for Fluid Interfaces, *Ann. Rev. Fluid Mech.*, vol. **35**, pp. 341–372, 2003.
- Shojaei, A., Ghaffarian, S. R., and Karimian, S. M. H., Modeling and Simulation Approaches in the Resin Transfer Molding Process: A Review, *Polym. Compos.*, vol. **24**, pp. 525–544, 2003.
- Tan, H. and Pillai, K. M., Effect of Fiber-Mat Anisotropy on 1D Filling in LCM: A Numerical Investigation, *Polym. Compos.*, vol. **29**, pp. 869–882, 2008.
- Tezduyar, T. E., Finite Element Method for Flow Problems with Moving Boundaries and Interfaces, *Arch. Comput. Methods Eng.*, vol. **8**, pp. 83–130, 2001.
- Toy, M. S., Surface Tension and Viscosity Studies of Molten Resins for Thermoplastic Recording, *J. Appl. Polym. Sci.*, vol. **9**, pp. 1593–1598, 1965.
- Trochu, F., Gauvin, R., and Gao, O. M., Numerical Analysis of the Resin Transfer Molding Process by the Finite Element Method, *Adv. Polym. Technol.*, vol. **12**, pp. 329–342, 1993.
- Trochu, F., Ruiz, E., Achim, V., and Soukane, S., Advanced Numerical Simulation of Liquid Composite Molding for Process Analysis and Optimization, *Composites A*, vol. **37**, pp. 890–902, 2006.
- Vafai, K. and Tien, C. L., Boundary and Inertia Effects on Flow and Heat Transfer in Porous Media, *Int. J. Heat Mass Transfer*, vol. **24**, pp. 195–203, 1981.
- Young, W. B. and Lai, C. L., Analysis of the Edge Effect in Resin Transfer Molding, *Composites A*, vol. **28A**, pp. 817–822, 1997.